# Intralayer doping effects on the high-energy magnetic correlations in NaFeAs

Jonathan Pelliciari,[1,*] Yaobo Huang,[1,2] Tanmoy Das,[3] Marcus Dantz,[1] Valentina Bisogni,[1,4] Paul Olalde Velasco,[1,†]
Vladimir N. Strocov,[1] Lingyi Xing,[2] Xiancheng Wang,[2] Changqing Jin,[2,5] and Thorsten Schmitt[1,‡]

[1]*Department of Synchrotron Radiation and Nanotechnology, Paul Scherrer Institut, CH-5232 Villigen PSI, Switzerland*
[2]*Beijing National Laboratory for Condensed Matter Physics, Institute of Physics, Chinese Academy of Sciences,*
*P.O. Box 603, Beijing 100190, China*
[3]*Department of Physics, Indian Institute of Science, Bangalore 560012, India*
[4]*National Synchrotron Light Source II, Brookhaven National Laboratory, Upton, New York 11973, USA*
[5]*Collaborative Innovation Center for Quantum Matters, Beijing, China*

We have used resonant inelastic x-ray scattering (RIXS) and dynamical susceptibility calculations to study the magnetic excitations in $NaFe_{1-x}Co_xAs$ ($x = 0$, 0.03, and 0.08). Despite a relatively low ordered magnetic moment, collective magnetic modes are observed in parent compounds ($x = 0$) and persist in optimally ($x = 0.03$) and overdoped ($x = 0.08$) samples. Their magnetic bandwidths are unaffected by doping within the range investigated. High-energy magnetic excitations in iron pnictides are robust against doping and present irrespectively of the ordered magnetic moment. Nevertheless, Co doping slightly reduces the overall magnetic spectral weight, differently from previous studies on hole-doped $BaFe_2As_2$, where it was observed constant. Finally, we demonstrate that the doping evolution of magnetic modes is different for the dopants being inside or outside the Fe-As layer.

## I. INTRODUCTION

Superconductivity (SC) in iron pnictides emerges after doping a metallic antiferromagnet [1]. Proximity, competition, and even coexistence between antiferromagnetic ordering (AF) and SC have been observed in the phase diagram in many Fe pnictide systems, with others, such as LiFeAs and $KFe_2As_2$, not showing any ordering in the SC dome. Similar behavior is also seen in cuprates and heavy-fermion superconductors [2,3], leading to the unsolved puzzle on whether a static magnetic order is a prerequisite to unconventional SC, or dynamical spin fluctuations without preferential wave vector are essential for superconducting pairing, irrespective of magnetic order. Therefore, the experimental characterization of dynamical spin fluctuations is vital to confirm or dismantle such concepts. In this context, inelastic neutron scattering (INS) is at the forefront of research in the study of magnetic excitations in unconventional superconductors (see Refs. [4–7] and references therein). However, momentum-resolved experimental detection of magnetic modes above 90 meV still represents a challenging task. This has been overcome by resonant inelastic x-ray scattering (RIXS) employing resonances at absorption edges (such as Fe $L_{2,3}$ or Cu $L_{2,3}$) which increase the cross section by several orders of magnitudes compared to INS. Recently, RIXS has been used to successfully detect high-energy magnetic excitations in superconducting cuprates [8–14] and Fe pnictides [15]. Moreover, INS and RIXS techniques complement each other in their span of the reciprocal space, with RIXS probing around the $\Gamma$ point and INS measuring around the antiferromagnetic ordering vector point in the Brillouin zone [4,5,16,17].

Although the exact origin of magnetism in Fe pnictides has not been fully established, they usually present a sizable ordered magnetic moment ($\mu$) on the order of $\approx 1 \mu_B$ [18,19]. NaFeAs contrasts with other Fe pnictides because of its low $\mu$ (about $0.1 \mu_B$) which differs in value with the most studied $BaFe_2As_2$ ($\approx 1.1-1.3 \mu_B$) by an order of magnitude [18,19]. Nonetheless, NaFeAs shows AF ordering even though at lower $T_N$ ($\approx 45$ K vs $\approx 140$ K for NaFeAs and $BaFe_2As_2$, respectively) [18,20]. The source of such change in $T_N$ has been ascribed to the larger distance between the As and the Fe layer in NaFeAs that increases electronic correlations consequently affecting also the spin wave spectrum [21,22]. When Co atoms substitute Fe within the Fe-As layer, AF is suppressed and SC arises with a $T_C \approx 20$ K at optimal doping [19]. The significant increase of both quasiparticle scattering rate and bandwidth as a function of Co substitution, as seen by angle-resolved photoelectron spectroscopy, have been ascribed to the decrease of the Fe-As bond length due to doping. As a consequence Hund's coupling and electronic correlations decrease upon Co doping [23]. This, in turn, should affect the behavior of spin fluctuations likely connected with superconductivity [2,3].

Here, we report on the measurements of high-energy magnetic fluctuations in $NaFe_{1-x}Co_xAs$ samples with $x = 0.0$ (parent compound, Par), $x = 0.03$ (close to optimal doping, $T_c = 20$ K, Opt) and $x = 0.08$ (overdoped, $T_c = 6$ K, Over) by means of RIXS. The bandwidth of these spin excitations is similar for Par, Opt, and Over. The presence of magnetic modes along (1, 0) and (1, 1) reciprocal directions in all samples is striking, displaying the coexistence of these modes with SC and their persistence even for overdoped samples. The nature of these excitations has been compared to self-consistent calculations of dynamical spin ($\chi_S$) and charge ($\chi_C$) susceptibilities by including the self-energy correction due to coupling of these modes to the electronic structure [24]. Our calculations show the dominance of $\chi_S$ over $\chi_C$. The experimental spectral weight of the magnetic modes is qualitatively observed to decrease when Co doping is increased.

---

*jonathan.pelliciari@psi.ch
†Present address: Instituto de Ciencias Nucleares, UNAM, Circuito Exterior, Ciudad Universitaria, 04510 Mexico D.F., Mexico.
‡thorsten.schmitt@psi.ch

## II. EXPERIMENTAL AND METHODS

### A. Samples preparation

Single crystals of $NaFe_{1-x}Co_xAs$ were grown by the self-flux method, using NaAs as the flux. The precursor $Na_3As$ was obtained by mixing Na lump and As powder, which were then sealed in an evacuated titanium tube and sintered at $650\,°C$ for 10 h. $Fe_{1-x}Co_xAs$ precursors were prepared by mixing Fe, Co, and As powder thoroughly, pressed into pellets, and sealed in an evacuated quartz tube, before being sintered at $700\,°C$ for 20 h. To ensure the homogeneity of the product, these pellets were ground and sintered another time. The stoichiometric amount of $Na_3As$, $Fe_{1-x}Co_xAs$, and As powder were weighed according to the element ratio of $Na(Fe_{1-x}Co_x)_{0.3}As$. The mixture was ground and put into an alumina crucible and sealed in a Nb crucible under 1 atm of argon gas. The Nb crucible was then sealed in an evacuated quartz tube and heated to $900\,°C$ before being slowly cooled down to $600\,°C$ ($3\,°C/h$) to grow single crystals. All sample preparations, except for sealing, were carried out in a glove box filled with high-purity argon gas. The element composition of the $NaFe_{1-x}Co_xAs$ single crystals was checked by energy-dispersive x-ray spectroscopy (EDS). Samples were stored in a sealed quartz tube and prepared for spectroscopic studies in a glove box under high-purity $N_2$ flow to avoid contact with air.

### B. Experimental conditions

The samples were mounted with the *ab* plane perpendicular to the scattering plane and the *c* axis lying in it [sketch in Fig. 1(b)] and postcleaved *in situ* at a pressure better than $2.0 \times 10^{-10}$ mbar. The reciprocal space directions studied are (1, 0) and (1, 1) according to the orthorhombic unfolded crystallographic notation [25]. The values of momentum transferred are expressed as relative lattice units (R.L.U.) ($q_{//} \times a/2\pi$). We use the convention of 1 Fe per unit cell. All the measurements were carried out at 13 K by cooling the manipulator with liquid helium. X-ray absorption spectra (XAS) and RIXS experiments were performed at the ADRESS beamline of the Swiss Light Source, Paul Scherrer Institute,

Villigen PSI, Switzerland [26,27]. XAS spectra were measured in total fluorescence yield (TFY). We measured Fe $L_{2,3}$ XAS spectra for all samples at $65°$ incidence angle relative to the sample surface. The RIXS spectrometer was set to a scattering angle of $130°$ and the incidence angle on the sample's surface was varied to change the in-plane momentum transferred ($q$) from (0, 0) to (0.44, 0) and from (0, 0) to (0.32, 0.32) as shown in the sketch of Fig. 1(b). All measurements in the present paper are recorded in grazing emission configuration [Fig. 1(b)]. The zero energy loss in our RIXS spectra has been estimated measuring spectra in $\sigma$ polarization. The total energy resolution has been measured employing the elastic scattering of carbon-filled acrylic tape and is around 110 meV.

### C. Calculations

We performed dynamical spin ($\chi_S$) and charge ($\chi_C$) susceptibility calculations. The calculations self-consistently include the many-body corrections within a random-phase approximation (RPA) as well as the self-energy correction due to both the spin and charge fluctuations starting from the DFT band structure [24]. The calculation includes intra- and interorbital Hubbard $U$, as well as Hund's coupling and pair-hopping interactions [28]. The doping effect is modeled by rigid band shift. The bare values of both $\chi_S$ and $\chi_C$, without including the self-energy correction, overestimate the energy scales and underestimate the weights of the collective excitations. The inclusion of the self-energy due to the coupling of the spin and charge fluctuations to the electronic state renormalizes the quasiparticle bands by about 30%, in accordance with various photoemission data [23,29]. This self-consistent approach has been successfully applied to describe the role of renormalized spin and charge excitations on superconductivity in cuprates [24] and heavy-fermion [30] and transition-metal dichalcogenide superconductors [31].

## III. RESULTS AND DISCUSSION

Figure 1(a) displays the Fe $L_{2,3}$ XAS spectra of Par, Opt, and Over, respectively collected at $65°$ incidence angle. The spectra are composed of a broad peak centered at 707 eV,
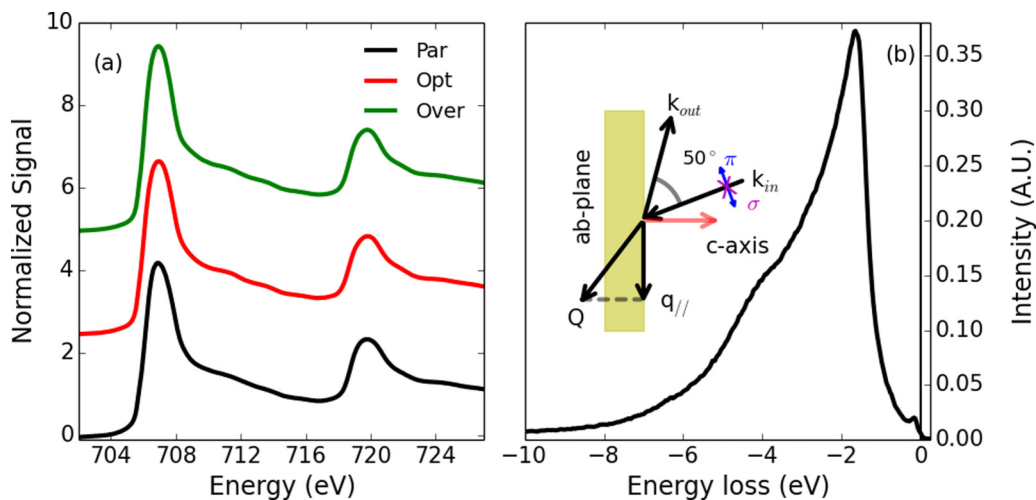


FIG. 1. (a) Fe $L_{2,3}$ x-ray absorption spectra for Par (black line), Opt (red line), and Over (green line). (b) Experimental configuration and Fe $L_3$ RIXS spectra for Par at (0.44, 0) and $h\nu_{in} = 707.3$ eV.
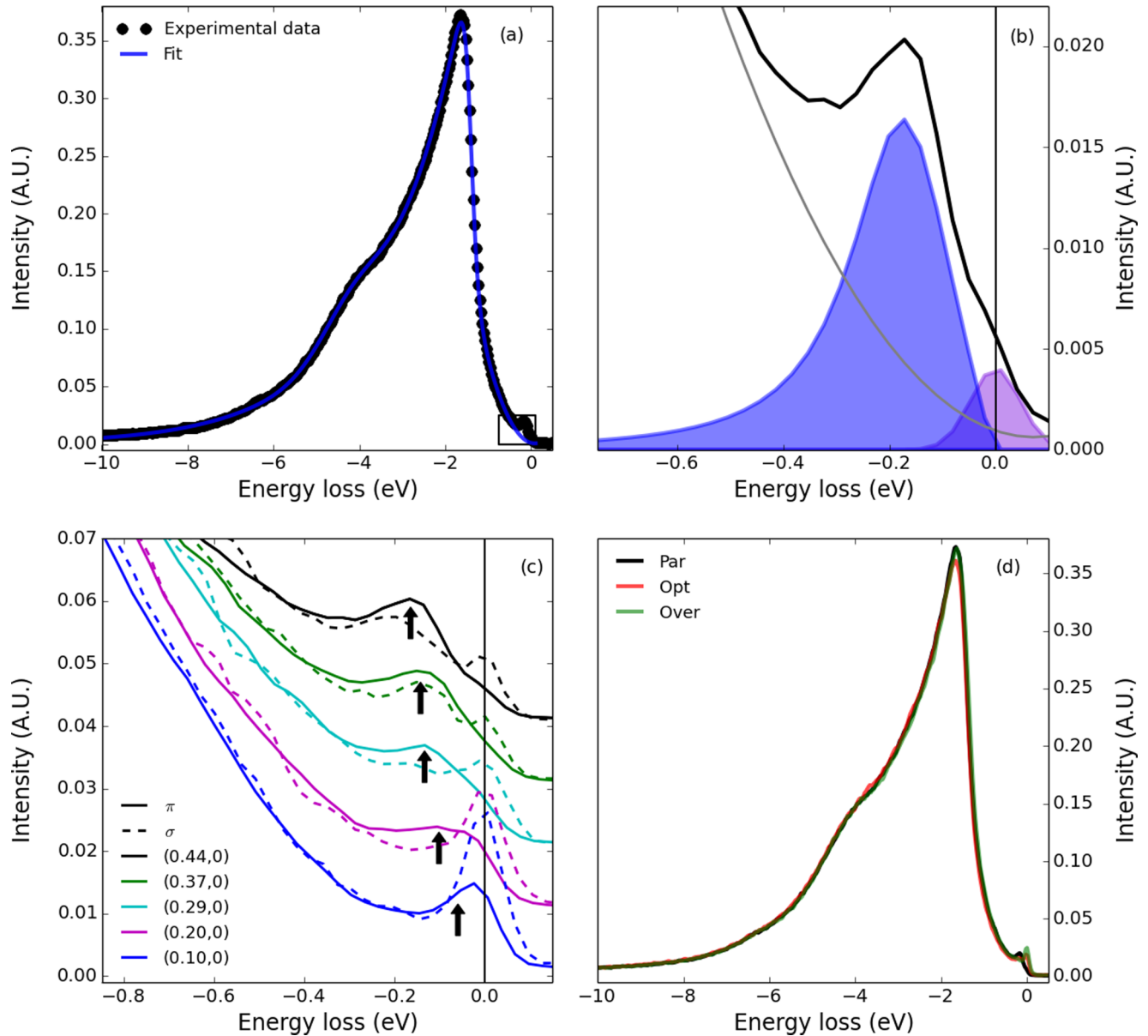
FIG. 2. (a) Experimental data (black dots) and relative fitting (blue solid line) of resonant emission of Par at (0.44, 0) and $\pi$ polarization. The incoming energy was tuned on the maximum of the Fe $L_3$ XAS. (b) Zoom into the low-energy-loss region of (a) and fitting of background (gray solid line), elastic (pink shaded), and magnetic peak (purple shaded). (c) Momentum and polarization dependence of the RIXS spectra of Par along $(0,0) \rightarrow (0.44,0)$. Solid line is $\pi$ polarization and dashed line is $\sigma$ polarization. (d) Comparison of RIXS spectra at (0.44, 0) and $\pi$ polarization for Par, Opt, and Over. All the data were collected at 13 K.

typical of metallic systems containing iron [15,32,33]. The incident energy for RIXS was tuned at the main Fe $L_3$ peak. In Fig. 1(b) an exemplary RIXS spectrum of Par at $q = (0.44,0)$ is shown. The main line in this spectrum resembles emission from metallic systems, with a broad asymmetric peak displaying a maximum at around $-2$ eV in energy loss ($h\nu_{out} - h\nu_{in}$) arising from resonant emission of itinerant electrons [15,32,34]. Normalization of the spectra is carried out integrating the area between $-0.4$ eV and $-10.0$ eV. This spectral region refers directly to the amount of Fe in the samples due to the element sensitivity of RIXS allowing direct comparison of samples despite different Fe content.

For the Par sample at (0.44, 0), a clear peak is observed at about 150 meV as shown in Figs. 2(a) and 2(b). We have tracked down this peak as a function of $q$ and incoming beam polarization [$\sigma$ and $\pi$, as defined in Fig. 1(b)]. Figure 2(c) shows the strong dispersive nature of the peak along the (1, 0) direction with the peak position displaying maximum energy at high $q$ transferred and decreasing moving towards the $\Gamma$ point, where it merges to the elastic line and is no longer resolved. A similar pattern is observed also along $(0,0) \rightarrow (0.32,0.32)$ (as shown in Fig. 3). This dispersive mode is ascribed to spin excitations in line with what is observed by INS on parent NaFeAs [22]. From polarization studies we observed that an incoming beam with $\pi$ polarization maximizes the spin
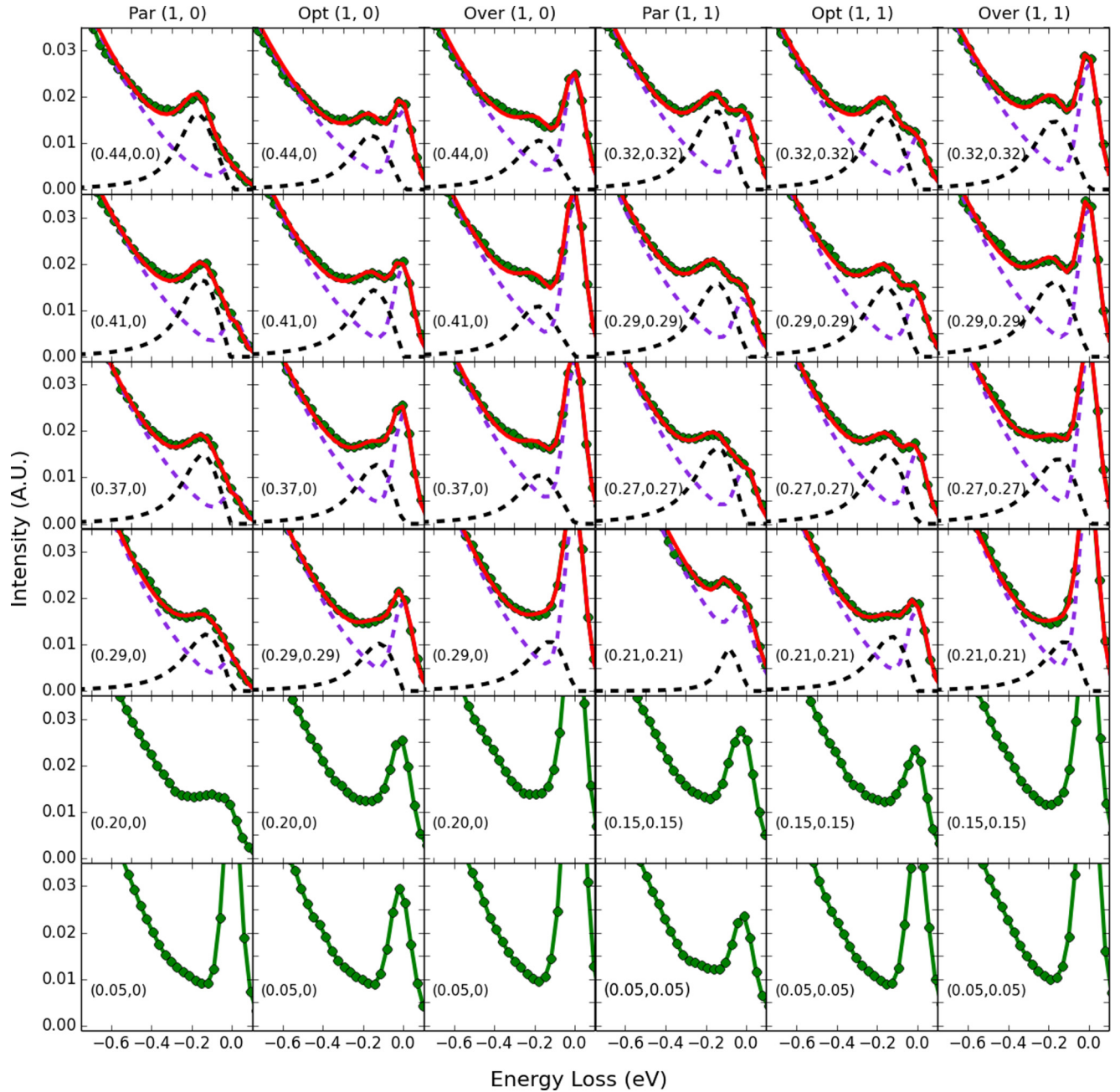
FIG. 3. Momentum dependence of RIXS spectra along $(0,0) \rightarrow (0.44,0)$ and $(0,0) \rightarrow (0.32,0.32)$ for Par, Opt, and Over. Spectra are recorded in $\pi$ polarization at the maximum of the Fe $L_3$ absorption edge. We show experimental data (green dots), background and elastic (purple dotted line), and magnetic peaks (black dotted line). The sum of background, elastic, and magnetic peaks is depicted as a red solid line. At low $q_{//}$ a fitting is unreliable, so no fitting was attempted.

excitations while minimizing the elastic line [Fig. 2(c)]. The reduction of the elastic channel in $\pi$ polarization is known in scattering theory [35] and the polarization was therefore selected accordingly.

Considering the low $\mu$ estimated by neutron scattering experiments [18,20], the detection of magnetic excitations in Par is remarkable, highlighting the high sensitivity of RIXS to fluctuating, rather than static, magnetic moments. A phenomenological comparison with INS data from Ref. [22] confirms the magnetic nature of the mode detected in Par, ruling out the appearance of sharp electron-hole pair excitations.

In Fig. 2(a), we show a typical fitting of the full emission line. The fitting analysis has been carried out similarly to what is described in Ref. [34] employing the following formulas:

$$I_{\text{fit}} = (\beta x^2 + \alpha x + c)(1 - g_\gamma) + I_0 \exp(ax)g_\gamma + G$$

with

$$g_\gamma = \left[ \exp\left(\frac{x + \omega^*}{\Gamma}\right) + 1 \right]^{-1}$$
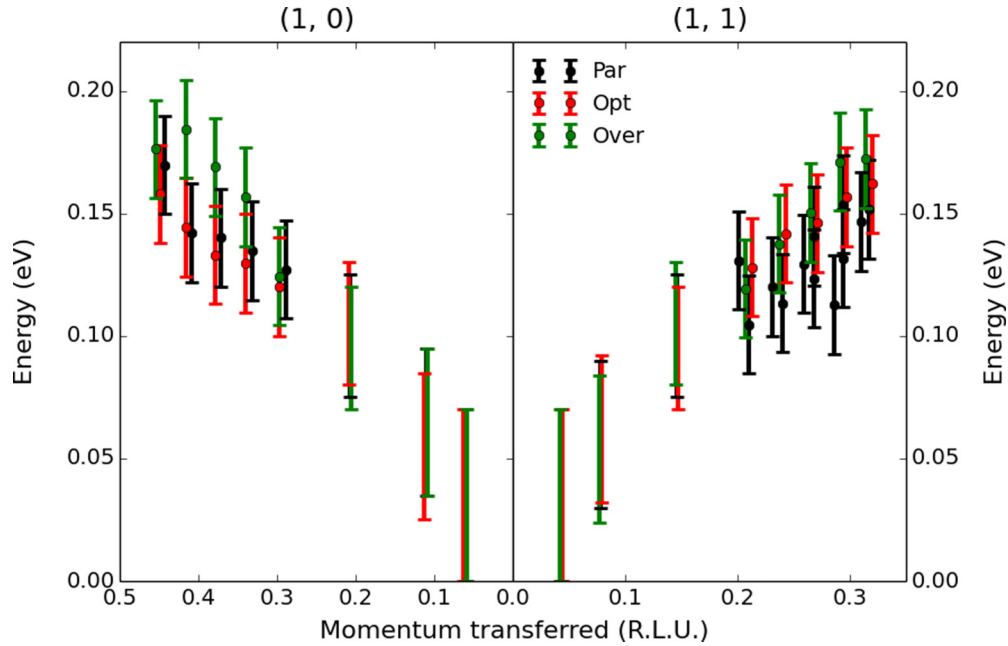
FIG. 4. Energy dispersion curves for Par, Opt, and Over vs transferred momentum. Left panel: (1, 0) direction; right panel: (1, 1) direction. At $q = 0.06$, $0.11$, and $0.2$ along (1, 0) and $q = 0.04$, $0.08$, and $0.15$ along (1, 1) the fitting was not possible because of overlap of the magnetic peak with the elastic line. Only an estimation of the energy range is provided for these values, as depicted by error bars. The points have been slightly shifted along the $x$ axis for better visualization.

and

$$ G = \frac{A}{\sigma\sqrt{2\pi}} \exp\left(\frac{(x+x_0)^2}{2\sigma^2}\right). $$

This approach fits the low values of energy loss ($x$) with a polynomial that is changed to exponential decay at higher values of energy loss. The crossover between the two regions is obtained employing the function $g_\Gamma$, having the energy $\omega^*$ and the width $\Gamma$ as parameters [34]. To better fit the the low-energy part of the background, we employ a second-order polynomial instead of the linear term proposed by Ref. [34]. This correction can be explained in the framework of the Mahan–Nozieres–De Dominicis model [36–39] as arising from many-body effects happening during absorption and emission of a resonant photon in metallic systems. An additional Gaussian term (introduced as $G$) has been introduced to fit the high-energy shoulder of the main emission line observed at $-4.5$ eV. This spectroscopic signature was not observed in tellurides [34] but it seems to be common in pnictides as shown by Refs. [15,33]. The result of this fitting analysis is plotted in Figs. 2(a) and 2(b) for Par at (0.44, 0).

In Fig. 2(d), we show the full RIXS spectra acquired for Par, Opt, and Over at (0.44, 0) with $\pi$ polarization and $h\nu = 707$ eV. The main emission line, centered at $-2$ eV, is similar for Par, Opt, and Over. This allows us to employ reliably the same fitting procedure for all the samples, confirming that the background has a similar slope in all the samples. Figure 3 shows the low-energy range of the RIXS spectra acquired for Par, Opt, and Over along $(0,0) \rightarrow (0.44,0)$ and $(0,0) \rightarrow (0.32,0.32)$. As in Ref. [15], we employed a resolution-limited Gaussian curve to fit the elastic line and an antisymmetrized Lorentzian for the magnetic peak. The reason for the use of a Lorentzian shape is due to the coupling of spin modes

to the Stoner continuum as observed in pnictides and doped cuprates [9–12,15,40] (see also Supplemental Material [41]). The elastic line intensity is observed to gradually increase from Par to Opt and then to Over. We believe that this enhancement is not linked to surface or sample quality but to a real increase of diffuse scattering arising from the Fe replacement by Co.

The bandwidth of magnetic excitations of NaFeAs is renormalized to lower values compared with AF BaFe$_2$As$_2$, as suggested by the lower $T_N$ [15,22]. Moving to doped samples, we discuss the main result of this work: the persistence of dispersive spin excitations in both optimal and overdoped samples (Fig. 3). The peaks ascribed above to magnetic excitations for Par are still present at $(0,0) \rightarrow (0.44,0)$ and $(0,0) \rightarrow (0.32,0.32)$ in both doped samples as depicted in the raw data Fig. 3 and in the fitting results of Fig. 4. Their line shape is conserved despite the large amount of Fe being substituted by Co (8% in the overdoped sample). Furthermore, the energy of the dispersion curves does not display significant modification between the samples as shown in Fig. 4, where the energies resulting from the fitting are summarized. Since Opt is not magnetically ordered, but superconducting, we reveal the coexistence of spin fluctuations with Cooper pairs. This entails an at least partially localized nature of the spins in NaFe$_{1-x}$Co$_x$As and a sizable magnetic coupling in the superconducting phase. Moreover, the presence of spin excitations in the Over sample is even more astonishing than in Opt, since the high doping level is far away from AF and at the end of the superconducting dome making spin fluctuations unexpected in this region of the phase diagram. Because of high intralayer doping a possible explanation for this can be assigned to randomness and dilution of AF bonds. Similar arguments have been employed in electron-doped cuprates to explain the hardening of spin excitations [42].
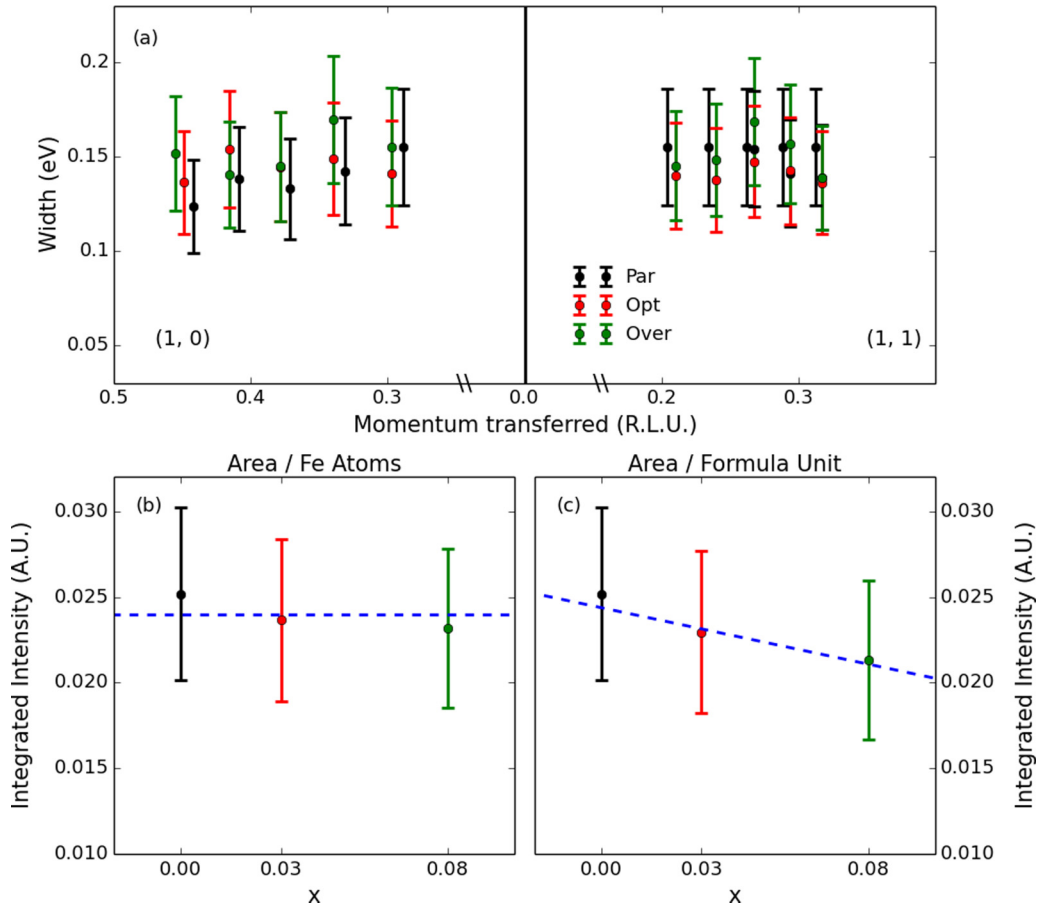
FIG. 5. (a) Fitting results. Widths of magnetic peaks vs transferred momentum. Left side: (1, 0) direction; right side: (1, 1) direction. (b) Sum of the area of magnetic peaks for (0.44, 0), (0.41, 0), (0.37, 0), (0.32, 0.32), (0.29, 0.29), and (0.27, 0.27) normalized to Fe content vs doping ($x$). (c) Sum of the area of magnetic peaks for (0.44, 0), (0.41, 0), (0.37, 0), (0.32, 0.32), (0.29, 0.29), and (0.27, 0.27) rescaled per formula unit vs doping ($x$). These peaks were selected because they are the most clear and with the highest intensity. The blue dotted lines represent a guide for the eye.

In Fig. 5(a) we display the width of the magnetic excitations' peak. In all compounds the peaks are broader than the experimental resolution indicating a mixing of spin excitations with the Stoner continuum [43]. We do not observe further broadening of magnetic peaks upon doping [Fig. 5(a)]. This indicates that the damping of such quasiparticles is unaffected by modification of Fermi surface topology, chemical potential, and scattering rate caused by doping [23]. To quantify the intensity, we integrated the magnetic peaks and summed the highest $q$ points. We employed the values obtained at $q_{//} = $ (0.44,0), (0.41, 0), (0.37, 0), (0.32, 0.32), (0.29, 0.29), and (0.27, 0.27). In these spectra, the peaks are well resolved from the elastic line and the intensity is maximal. Since we normalized to the Fe fluorescence line, the intensity can be interpreted as the magnetic weight per Fe atom. The results in Fig. 5(b) show that the magnetic weight per Fe atom is preserved [Fig. 5(b)] after doping, indicating magnetism residing on Fe atoms. Nonetheless, the Fe content decreases upon doping (Co replaces Fe), thus decreasing the absolute RIXS signal. This implies that the magnetic spectral weight has to be rescaled to the overall formula unit [multiplying by the relative factors (1−0.03) and (1−0.08) for Opt and Over, respectively]. This renormalization slightly reduces the

integrated intensity of spin excitations due to dilution of Fe by Co [see Figs. 5(b) and 5(c)].

To further elucidate the experimental data, we calculated the dynamical susceptibility for all the samples. The self-energy dressed $\chi_S$ and $\chi_C$ were disentangled as displayed in the color plot in Fig. 6. Our calculations show that the intensity of $\chi_S$ is almost an order of magnitude higher than $\chi_C$, and the latter is pushed slightly higher in energy than the former. This is due to electronic correlations that shift the spectral weight of charge modes to higher energies leaving the spin part to reside at lower energies. Comparison of $\chi_S$ along the (1, 0) and (1, 1) directions clearly reveals that the spin modes are more pronounced at (1, 0). The large $\chi_S$ around (1, 0) is the residual of AF ordering, indicating the ability of theory to catch the tendency towards AF ordering with underdoping. As RIXS is sensitive to the dynamical susceptibility [17], we confirm that the main spectroscopic weight detected in the low-energy region (<200 meV) after background subtraction in NaFe$_{1−x}$Co$_x$As is mainly of magnetic origin. This comparison between experiments and calculations is carried out on a qualitative basis because calculations involving matrix element effects and the presence of a core hole in the intermediate state of the RIXS process should be included to quantitatively
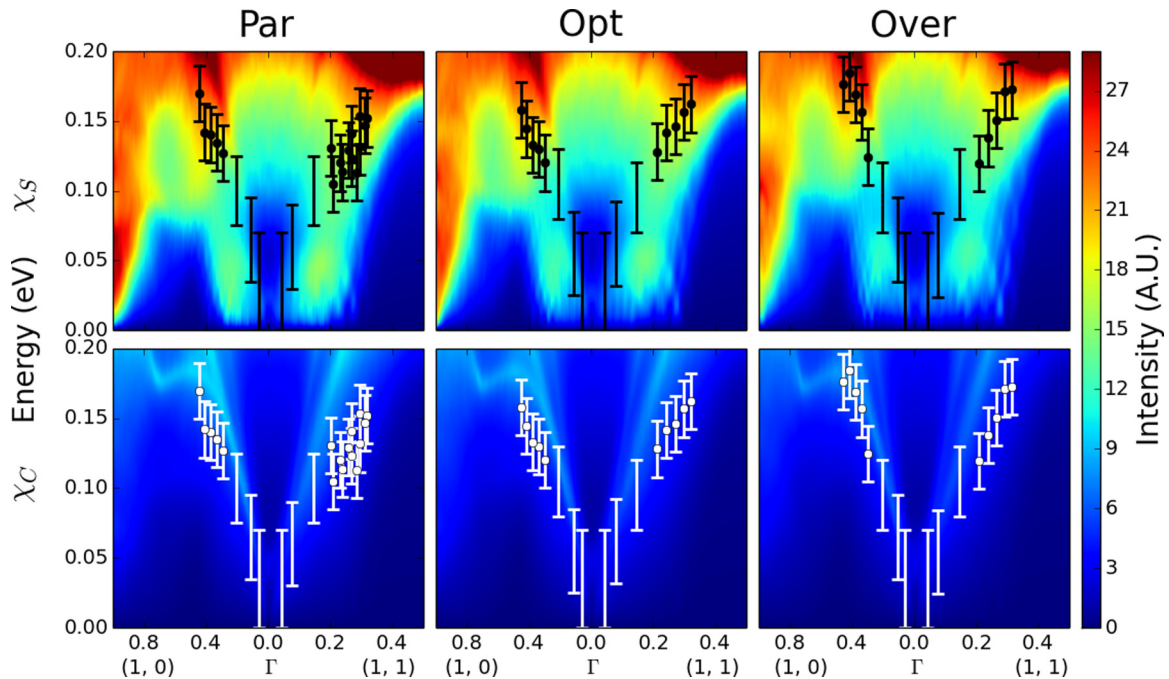
FIG. 6. Calculated dynamical susceptibility (color plot) overlaid with experimental data (black and white dots with error bars) for Par, Opt, and Over. Top row: Calculated spin susceptibility ($\chi_S$). Bottom row: Calculated charge susceptibility ($\chi_C$). Both crystallographic directions (1, 0) and (1, 1) are shown.

compare $\chi$ calculations with the experimental RIXS intensity. Our calculations for the same Co doping levels as measured display that doping slightly shifts the spin modes upwards in energy. Comparing experimental data (dots in Fig. 6) and calculations (color plot in Fig. 6) we find that the extracted dispersions follow the highest intensity region of the calculated $\chi_S$. The small hardening of $\chi_S$ indicated by calculations has not been observed in our RIXS measurements, likely being beyond the resolving capacity of our current instrumentation. The decrease of spectral weight for increasing Co doping observed in our experiment is qualitatively captured by the calculations, as can be observed by the intensity color scale of Fig. 6. However, this comparison is not meant to be quantitative since in the calculations the matrix elements have not been taken into account.

The phenomenological agreement of the energy of spin excitations in theory and experiment confirms the robustness of spin excitations in NaFe$_{1-x}$Co$_x$As even when a large amount of Fe has been substituted by Co. In high-$\mu$ Fe pnictides, such as the BaFe$_2$As$_2$ series, the energy of magnetic correlations for BaFe$_{2-x}$Ni$_x$As$_2$ and Ba$_{0.6}$K$_{0.4}$Fe$_2$As$_2$ is, relatively to the parent compound, unchanged and softened, respectively [15,44,45]. This illustrates that the evolution of spin fluctuations is affected by doping site (inside or outside the Fe layer) and type of carriers (electrons or holes). These observations demonstrate that the presence of a sizable magnetic coupling seems to be universal, whereas its evolution with doping is not.

## IV. CONCLUSIONS

In conclusion, we have performed RIXS measurements and DFT-based calculations of dynamic susceptibilities on low-static-$\mu$ NaFe$_{1-x}$Co$_x$As ($x = 0$, 0.03, and 0.08). We observe broad and dispersive spin excitations around 150 meV from

$(0,0) \rightarrow (0,0.44)$ and $(0,0) \rightarrow (0.32,0.32)$ in all the samples measured. In AF NaFeAs the spin excitations, remarkably, manifest themselves despite its low $\mu$. This confirms the quantum fluctuating nature of spins in NaFeAs and demonstrates the ability of RIXS to probe spin correlations in low-$\mu$ itinerant systems. In the optimally doped samples, magnetic ordering is replaced by SC with spin correlations surviving and preserving their bandwidth. Measurements on the overdoped compound reveal the presence of magnetic modes also when SC has been suppressed and a metallic phase has taken over. The spectral weight of such modes seems to gradually decrease with Co doping. Our experiments demonstrate that the suppression of SC is not linked with a complete disappearance of high-energy magnetic excitations, as magnetic coupling is present also in overdoped samples, but is rather connected to subtle effects likely happening at lower energy scale.

[1] Y. Kamihara, T. Watanabe, M. Hirano, and H. Hosono, J. Am. Chem. Soc. **130**, 3296 (2008).

[2] D. J. Scalapino, Rev. Mod. Phys. **84**, 1383 (2012).

[3] A. Chubukov, Annu. Rev. Condens. Matter Phys. **3**, 57 (2012).

[4] J. M. Tranquada, G. Xu, and I. A. Zaliznyak, J. Magn. Magn. Mater. **350**, 148 (2014).

[5] P. Dai, Rev. Mod. Phys. **87**, 855 (2015).

[6] D. S. Inosov, C. R. Phys. **17**, 60 (2015).

[7] M. Fujita, H. Hiraka, M. Matsuda, M. Matsuura, J. M. Tranquada, S. Wakimoto, G. Xu, and K. Yamada, J. Phys. Soc. Jpn. **81**, 011007 (2011).

[8] M. P. M. Dean, R. S. Springell, C. Monney, K. J. Zhou, J. Pereiro, I. Boovi, B. Dalla Piazza, H. M. Rønnow, E. Morenzoni, J. van den Brink, T. Schmitt, and J. P. Hill, Nat. Mater. **11**, 850 (2012).

[9] M. Le Tacon, G. Ghiringhelli, J. Chaloupka, M. M. Sala, V. Hinkov, M. W. Haverkort, M. Minola, M. Bakr, K. J. Zhou, S. Blanco-Canosa, C. Monney, Y. T. Song, G. L. Sun, C. T. Lin, G. M. De Luca, M. Salluzzo, G. Khaliullin, T. Schmitt, L. Braicovich, and B. Keimer, Nat. Phys. **7**, 725 (2011).

[10] W. S. Lee, J. J. Lee, E. A. Nowadnick, S. Gerber, W. Tabis, S. W. Huang, V. N. Strocov, E. M. Motoyama, G. Yu, B. Moritz, H. Y. Huang, R. P. Wang, Y. B. Huang, W. B. Wu, C. T. Chen, D. J. Huang, M. Greven, T. Schmitt, Z. X. Shen, and T. P. Devereaux, Nat. Phys. **10**, 883 (2014).

[11] K. Ishii, M. Fujita, T. Sasaki, M. Minola, G. Dellea, C. Mazzoli, K. Kummer, G. Ghiringhelli, L. Braicovich, T. Tohyama, K. Tsutsumi, K. Sato, R. Kajimoto, K. Ikeuchi, K. Yamada, M. Yoshida, M. Kurooka, and J. Mizuki, Nat. Commun. **5**, 3714 (2014).

[12] Y. Y. Peng, M. Hashimoto, M. M. Sala, A. Amorese, N. B. Brookes, G. Dellea, W.-S. Lee, M. Minola, T. Schmitt, Y. Yoshida, K.-J. Zhou, H. Eisaki, T. P. Devereaux, Z.-X. Shen, L. Braicovich, and G. Ghiringhelli, Phys. Rev. B **92**, 064517 (2015).

[13] M. Minola, G. Dellea, H. Gretarsson, Y. Y. Peng, Y. Lu, J. Porras, T. Loew, F. Yakhou, N. B. Brookes, Y. B. Huang, J. Pelliciari, T. Schmitt, G. Ghiringhelli, B. Keimer, L. Braicovich, and M. Le Tacon, Phys. Rev. Lett. **114**, 217003 (2015).

[14] L. Braicovich, J. van den Brink, V. Bisogni, M. M. Sala, L. J. P. Ament, N. B. Brookes, G. M. De Luca, M. Salluzzo, T. Schmitt, V. N. Strocov, and G. Ghiringhelli, Phys. Rev. Lett. **104**, 077002 (2010).

[15] K.-J. Zhou, Y.-B. Huang, C. Monney, X. Dai, V. N. Strocov, N.-L. Wang, Z.-G. Chen, C. Zhang, P. Dai, L. Patthey, J. van den Brink, H. Ding, and T. Schmitt, Nat. Commun. **4**, 1470 (2013).

[16] M. P. M. Dean, J. Magn. Magn. Mater. **376**, 3 (2015).

[17] L. J. P. Ament, M. van Veenendaal, T. P. Devereaux, J. P. Hill, and J. van den Brink, Rev. Mod. Phys. **83**, 705 (2011).

[18] D. C. Johnston, Adv. Phys. **59**, 803 (2010).

[19] G. R. Stewart, Rev. Mod. Phys. **83**, 1589 (2011).

[20] S. Li, C. de la Cruz, Q. Huang, G. F. Chen, T.-L. Xia, J. L. Luo, N. L. Wang, and P. Dai, Phys. Rev. B **80**, 020504 (2009).

[21] Z. P. Yin, K. Haule, and G. Kotliar, Nat. Mater. **10**, 932 (2011).

[22] C. Zhang, L. W. Harriger, Z. Yin, W. Lv, M. Wang, G. Tan, Y. Song, D. L. Abernathy, W. Tian, T. Egami, K. Haule, G. Kotliar, and P. Dai, Phys. Rev. Lett. **112**, 217202 (2014).

[23] Z. R. Ye, Y. Zhang, F. Chen, M. Xu, J. Jiang, X. H. Niu, C. H. P. Wen, L. Y. Xing, X. C. Wang, C. Q. Jin, B. P. Xie, and D. L. Feng, Phys. Rev. X **4**, 031041 (2014).

[24] T. Das, R. S. Markiewicz, and A. Bansil, Adv. Phys. **63**, 151 (2014).

[25] J. T. Park, D. S. Inosov, A. Yaresko, S. Graser, D. L. Sun, P. Bourges, Y. Sidis, Y. Li, J.-H. Kim, D. Haug, A. Ivanov, K. Hradil, A. Schneidewind, P. Link, E. Faulhaber, I. Glavatskyy, C. T. Lin, B. Keimer, and V. Hinkov, Phys. Rev. B **82**, 134503 (2010).

[26] V. N. Strocov, T. Schmitt, U. Flechsig, T. Schmidt, A. Imhof, Q. Chen, J. Raabe, R. Betemps, D. Zimoch, J. Krempasky, X. Wang, M. Grioni, A. Piazzalunga, and L. Patthey, J. Synchrotron Radiat. **17**, 631 (2010).

[27] G. Ghiringhelli, A. Piazzalunga, C. Dallera, G. Trezzi, L. Braicovich, T. Schmitt, V. N. Strocov, R. Betemps, L. Patthey, X. Wang, and M. Grioni, Rev. Sci. Instrum. **77**, 113108 (2006).

[28] Intraorbital $U = 2.6$ eV for $d_{xz/yz}$, 1.45 eV for $d_{xy}$, 3 eV for $d_{x^2-y^2}$, and 1.8 eV for $d_{z^2}$ orbitals. The interorbital $U$ is 2 eV, and Hund's coupling ($J$) is 1 eV, while pair-hopping interaction is 0.5 eV for all orbitals (averaged). These values are obtained from the Kanamori criterion such that the corresponding renormalized imaginary part of the spin susceptibilities remains positive. The absolute value of $J$ is model-dependent since different methods use different sets of interaction diagrams. In our method, the self-energy correction is feedback to the electronic structure. Therefore, it automatically enhances the value of $J$. Our value of $J = 1$ eV is comparable to that of similar methods such as DMFT ($J = 0.8$ eV) [21] and FLEX ($J = 1$ eV) [46]. This value is reduced in a simple RPA approach ($J = 0.5$ eV) [47].

[29] M. Yi, D. H. Lu, R. G. Moore, K. Kihou, C.-H. Lee, A. Iyo, H. Eisaki, T. Yoshida, A. Fujimori, and Z.-X. Shen, New J. Phys. **14**, 073019 (2012).

[30] T. Das, J.-X. Zhu, and M. J. Graf, Phys. Rev. Lett. **108**, 017001 (2012).

[31] T. Das and K. Dolui, Phys. Rev. B **91**, 094510 (2015).

[32] E. Z. Kurmaev, J. A. McLeod, N. A. Skorikov, L. D. Finkelstein, A. Moewes, Y. A. Izyumov, and S. Clarke, J. Phys. Condens. Matter **21**, 345701 (2009).

[33] W. L. Yang, A. P. Sorini, C.-C. Chen, B. Moritz, W.-S. Lee, F. Vernay, P. Olalde-Velasco, J. D. Denlinger, B. Delley, J.-H. Chu, J. G. Analytis, I. R. Fisher, Z. A. Ren, J. Yang, W. Lu, Z. X. Zhao, J. van den Brink, Z. Hussain, Z.-X. Shen, and T. P. Devereaux, Phys. Rev. B **80**, 014508 (2009).

[34] J. N. Hancock, R. Viennois, D. van der Marel, H. M. Rønnow, M. Guarise, P.-H. Lin, M. Grioni, M. Moretti Sala, G. Ghiringhelli, V. N. Strocov, J. Schlappa, and T. Schmitt, Phys. Rev. B **82**, 020513(R) (2010).

[35] J. Als-Nielsen and D. McMorrow, *Elements of Modern X-ray Physics*, 2nd ed. (Wiley, U.K., 2011).

[36] P. Nozières and E. Abrahams, Phys. Rev. B **10**, 3099 (1974).

[37] T. Privalov, F. Gelmukhanov, and H. Agren, Phys. Rev. B **64**, 165116 (2001).

[38] G. D. Mahan, Phys. Rev. B **15**, 4587 (1977).

[39] C.-O. Almbladh, Phys. Rev. B **16**, 4343 (1977).

[40] M. P. M. Dean, G. Dellea, R. S. Springell, F. Yakhou-Harris, K. Kummer, N. B. Brookes, X. Liu, Y.-J. Sun, J. Strle, T. Schmitt, L. Braicovich, G. Ghiringhelli, I. Boovi, and J. P. Hill, Nat. Mater. **12**, 1019 (2013).

[41] See Supplemental Material at http://link.aps.org/supplemental/10.1103/PhysRevB.93.134515 for illustration of the asymmetry in the magnetic peaks.

[42] C. J. Jia, E. A. Nowadnick, K. Wohlfeld, Y. F. Kung, C.-C. Chen, S. Johnston, T. Tohyama, B. Moritz, and T. P. Devereaux, Nat. Commun. **5**, 3314 (2014).

[43] V. Stanev, J. Kang, and Z. Tesanovic, Phys. Rev. B **78**, 184509 (2008).

[44] H. Luo, X. Lu, R. Zhang, M. Wang, E. A. Goremychkin, D. T. Adroja, S. Danilkin, G. Deng, Z. Yamani, and P. Dai, Phys. Rev. B **88**, 144516 (2013).

[45] M. Wang, C. Zhang, X. Lu, G. Tan, H. Luo, Y. Song, M. Wang, X. Zhang, E. A. Goremychkin, T. G. Perring, T. A. Maier, Z. Yin, K. Haule, G. Kotliar, and P. Dai, Nat. Commun. **4**, 2874 (2013).

[46] Z.-J. Yao, J.-X. Li, and Z. D. Wang, New J. Phys. **11**, 025009 (2009).

[47] S. Graser, T. A. Maier, P. J. Hirschfeld, and D. J. Scalapino, New J. Phys. **11**, 025016 (2009).